CrossMark

RESEARCH ARTICLE

On the transition from strombolian to fountaining activity: a thermal energy-based driver

Maxime Bombrun[1,2,3,4] · Letizia Spampinato[5] · Andrew Harris[1,2] · Vincent Barra[3,4] · Tommaso Caltabiano[5]

Abstract Since 1999, Mount Etna's (Italy) South-East crater system has been characterised by episodic lava fountaining. Each episode is characterised by initial strombolian activity followed by transition to sustained fountaining to feed high-effusion rate lava flow. Here, we use thermal infrared data recorded by a permanent radiometer station to characterise the transition to sustained fountaining fed by the New South-East crater that developed on the eastern flank of the South-East crater starting from January 2011. We cover eight fountaining episodes that occurred between 2012 and 2013. We first developed a routine to characterise event waveforms apparent in the precursory, strombolian phase. This allowed extraction of a database for thermal energy and waveform shape for 1934 events. We detected between 66 and 650 events per episode, with event durations being between 4 and 55 s. In total, 1508 (78 %) of the events had short waxing phases and dominant waning phases. Event frequency increased as climax was approached. Events had energies of between 3.0×10^6 and 5.8×10^9 J, with rank order analysis indicating the highest possible event energy of 8.1×10^9 J. To visualise the temporal evolution of retrieved parameters during the precursory phase, we applied a dimensionality reduction technique. Results show that weaker events occur during an onset period that forms a low-energy "sink". The transition towards fountaining occurs at 10^7 J, where subsequent events have a temporal trend towards the highest energies, and where sustained fountaining occurs when energies exceed 10^9 J. Such an energy-based framework allows researchers to track the evolution of fountaining episodes and to predict the time at which sustained fountaining will begin.

Editorial responsibility: J. Taddeucci

Key points
• Strombolian activity parameterised through the transition to fountaining
• A database of 1934 events is provided
• Our data allow a better understanding of the strombolian-fountaining transition

✉ Maxime Bombrun
  bombrun@isima.fr

[1] Clermont-Université, Université Blaise Pascal, LMV, BP 10448, F-63000 Clermont-Ferrand, France

[2] CNRS, UMR 6524, LMV, F-63173 Aubiere, France

[3] Clermont-Université, Université Blaise Pascal, LIMOS, BP 10448, F-63000 Clermont-Ferrand, France

[4] CNRS, UMR 6158, LIMOS, F-63173 Aubiere, France

[5] Istituto Nazionale di Geofisica e Vulcanologia, Sezione di Catania, Osservatorio Etneo, Piazza Roma 2, 95125 Catania, Italy

Introduction

Lava fountains, erupted as part of "Hawaiian style" explosions, are a relatively weak form of volcanic explosive activity during which sustained jets of molten lava and gas are ejected at mass eruption rates of 10^5–10^6 kg/s over time periods of a few hours (e.g. Mercalli 1907; Newhall and Self 1982; Houghton and Gonnermann 2008). However, they are frequently occurring explosions which characterise activity at basaltic centres such as Mt. Etna and Hawaii (e.g. Heliker and Mattox 2003; Behncke et al. 2006; Stovall et al. 2010). They are capable of feeding tephra plumes to altitudes of up to several thousand metres (e.g. Swanson et al. 1979; Vergniolle and Mangan 2000; Wolff and Sumner 2000; Andronico et al. 2008), causing local air fall damage and presenting a hazard to

Springer

local air traffic operations (e.g. Andronico et al. 2008; Calvari et al. 2011). As a result, research and technology development has focused on understanding the trigger mechanisms for fountaining onset and the transition from milder strombolian events to sustained fountaining, as well as the geophysical waveforms associated with each phase (e.g. Allard et al. 2005; Vergniolle and Ripepe 2008; Calvari et al. 2011; Ganci et al. 2012, 2013; Gouhier et al. 2012; Bonaccorso et al. 2013a, b). The local hazard posed by fountaining episodes has also led to the development of geophysical methods to track event evolution in near-real time (Bonaccorso et al. 2011; Sciotto et al. 2011) and to set up alert systems (Ulivieri et al. 2013). Indeed, while the most efficient and quantitative way to track the onset and evolution of a fountaining episode in near-real time is through geophysical observations, plume emission dynamics can be tracked using ground-based thermal cameras and radiometers (see Ramsey and Harris (2013), Harris (2013) and Spampinato et al. (2015) for review). Satellite-based sensors can also be applied (e.g. Aloisi et al. 2002; Bertrand et al. 2003; Aksakal 2013) if the episode is sufficiently long-lasting, the satellite temporal resolution sufficiently high and the target cloud-free.

Radiometers have proved to be a particularly powerful tool for characterising explosive eruption styles (e.g. Harris and Ripepe 2007a; Harris et al. 2008; Sahetapy-Engel et al. 2008) and defining transitions between different explosive or degassing regimes (e.g. Marchetti and Harris 2008; Pioli et al. 2008; Marchetti et al. 2009), as well as for examining relations between explosion style and other system parameters (e.g. Harris et al. 1996; Ripepe et al. 2002, 2005; Spampinato et al. 2015). The advantage of radiometers is that they are inexpensive and are capable of high sampling rates while keeping data rates and processing requirements, to a minimum (e.g. Zettwoog and Tazieff 1972; Harris et al. 2005; Murè et al. 2013). The high sampling rates allow characterisation of explosion-related waveforms developing over time-scales of a few tenths of a second (e.g. Shimozuru 1971; Johnson et al. 2005; Ripepe and Harris 2008) and repeating at frequencies of just a few seconds to tens of seconds (e.g. Johnson et al. 2005; Harris and Ripepe 2007b; Branan et al. 2008). At the same time, the low cost of the instrument means that the radiometer can be left in unsafe areas, and any that are destroyed can be readily replaced (Harris et al. 2003; Ripepe et al. 2004; Spampinato et al. 2015). Limits mainly include weather conditions, with thick fog and/or ash fall preventing measurements over longer (>100 m) lines of sight. Waveform modification issues will also apply when considering signal changes that are shorter than the detector response time, but this tends to apply only to events shorter than 0.25 s (Harris 2013).

We here describe a low-cost radiometer system that was installed on Mt. Etna near the end of 2011 to track explosive activity at the SE Crater (SEC) and New SE Crater (NSEC); these sites are part of a system well known for its frequent lava

fountain activity (e.g. Bonaccorso et al. 2011; Calvari et al. 2011; Sciotto et al. 2011; Ganci et al. 2012; Behncke et al. 2014; Spampinato et al. 2015) (Fig. 1). We here use the term episode to describe a fountaining episode, which at Mt. Etna typically comprises three phases: a precursory strombolian phase, a sustained fountaining phase and a waning phase of intermittent strombolian activity during which lava flows stagnate and cool (Ganci et al. 2012). Episodes typically begin with discrete strombolian events that increase in frequency and intensity over a period of several hours to climax in sustained fountaining (e.g. Vergniolle and Ripepe 2008; Ulivieri et al. 2013; Calvari et al. 2011; Spampinato et al. 2015). As part of this precursory phase, Calvari et al. (2011) described an increase in the frequency of explosive and lava flow emission events in the 30 min before the transition to sustained fountaining. During this phase of "transitional eruptive style" (e.g. Parfitt and Wilson 1995; Parfitt 2004; Spampinato et al. 2008), events became "almost continuous" (Calvari et al. 2011). The transition to sustained fountaining then occurred over a period of just two minutes. As observed in Hawaii (Wolfe et al. 1988), the period of sustained fountaining can then die out over a timescale that is similarly short. Our data processing here focused on extracting event thermal energies during the phase of strombolian activity that comprises the build-up to sustained fountaining, which then feeds the highest ash plumes and high-effusion rate lava flows. Our aim was to discover if there were any trends in thermal energy that would allow us to predict the transition to sustained fountaining, which can be quite sudden. Our analysis reveals a systematic increase in event frequency and energy as the system evolves to fountaining; clear thermal energy thresholds are crossed as the system transitions from low-frequency strombolian activity, through high-frequency strombolian activity, to sustained jetting.

Fig. 1 Photograph showing one of the lava fountaining episodes fed by the Mt. Etna's New South-East crater since January 2011. Photo by Alessandro La Spina, 12 April 2012

Methodology

Mt. Etna was selected for this study because it is currently the most active volcano on Earth in terms of lava fountain activity. Eruptions occur both at the summit (3330 m above sea level), where currently there are four degassing craters, and from its flanks. Since 1999, the SEC, and now the NSEC, has been particularly active with hundreds of fountaining episodes recorded through 2014 (e.g. Harris and Neri 2002; Calvari et al. 2011; Behncke et al. 2014; Spampinato et al. 2015).

The instrument used in this study was a thermopile-based spot radiometer manufactured by Optris, the CTfast-LT15F (Fig. 2). This radiometer offers an extremely short response time of 6 ms and a temperature measurement range from −50 to 975 °C in the spectral region of 8–14 μm. The optical system has a resolution of 15:1, meaning that at a distance of 1050-m spectral radiance is integrated over a spot diameter of 70 m. Here, we used a sampling rate of 50 Hz allowing acquisition of a huge amount of data with a small memory requirement. This sampling rate corresponds to 3000 values per minute, which is equivalent to 24 kb per minute. The radiometer was also equipped with a small internal display allowing visualisation, in real time, of temperature (in Celsius) as well as voltage output. We here use apparent temperature, uncorrected for emissivity or atmospheric effects. However, emissivity should be close to one, and at this altitude (3000 m), atmospheric effects will be negligible over line-of-sight distances out to 1 km for high-temperature targets (Harris 2013).

The radiometer was set up at Belvedere site (EBEL, Fig. 3), from which the line-of-sight to NSEC was 1 km, so that the radiometer field of view (FOV) was circular with an area of ~3490 m². This FOV included the NSEC rim, but most of the FOV was clear sky. Considering the low-energy draw of the radiometer (~20 mA), power requirements and data logging needs were trivial (e.g. Harris et al. 2005; Murè et al. 2013).

Fig. 2 Radiometer setup at the EBEL station, monitoring at Mt. Etna. The station was destroyed by lava flows fed by the 28 February 2013 paroxysm

Data were collected automatically and transmitted via telemetry to the Osservatorio Etneo of Istituto Nazionale di Geofisica e Vulcanologia (Murè et al. 2013; Spampinato et al. 2015). This allowed near-real time tracking of the eight lava fountain episodes that occurred between 4 March 2012 and 28 February 2013 when EBEL station was buried by a lava flow (Spampinato et al. 2015).

To set waveforms collected during the precursory strombolian phase in context, we examined thermal data collected during normal explosive activity at Stromboli volcano (Italy). Stromboli's explosions are typically defined as weak but persistent bursts of incandescent ballistic ejecta (e.g. Patrick et al. 2007) and ash (e.g. Patrick 2007) to heights of up to a few hundred metres, in explosions lasted a few seconds and repeating at a rate of 13 explosions per hour (Harris and Ripepe 2007b; Ripepe et al. 2008). In 2012 and 2014, two campaigns were completed on Stromboli during which thermal cameras were used to acquire high-frame rate videos focusing on the explosive vent (Bombrun et al. 2015a, b) and a wider field of view to cover ascent of the whole plume (Harris et al. 2013a; Bombrun et al. 2015b). To obtain similar values to those obtained by the radiometer at Mt. Etna, we calculated the average temperature for a conic field of view (i.e. a circle in the 2D image) through time (Fig. 4) during seven explosions.

Algorithm

The objective of the algorithm was to temporally define a fountaining episode, a strombolian event and a strombolian explosion (Fig. 5). A single episode is composed of an ascension phase and a descent phase. Ascension begins with an initial jet that results in a waveform onset with a steep slope. An inflexion point may characterise the first burst phase, after which the apparent temperature increases more steeply to the climax (Harris and Ripepe 2007a; Sahetapy-Engel et al. 2008). The descent phase can consist of a steadily declining trend during which emission wanes if we record a single burst, or can be overprinted by new peaks if further bursts occur. In this case, we record a "thermal phenomenon" that is composed of multiple bursts which each generates a peak. After the last burst, a cooling curve is recorded, due to cooling ejecta on the cone outer flank between events (Harris et al. 2013b). To define an episode, we need to obtain times corresponding to each of its component phases. To do this, we used an algorithm based on the work of Bertrand et al. (2011).

We first considered the whole data set covering the entire lava fountain episode. Due to the huge amount of data, a first step was to reduce the number of values. In the case of the whole dataset, we iterated three times resampling at 1/10 of the original sample rate during each iteration. As a result, a sequence of 1,248,000 points will be reduced to 1248 points. The beginning (t_{beg}) and the end (t_{end}) of the entire data set are known and can be extracted directly. To extract individual

Fig. 3 Shaded relief map of Mt. Etna volcano. The *red rectangle* is our region of interest containing the location of Bocca Nuova (BN), Voragine (VOR), North-East Crater (NEC), South-East Crater (SEC) and the New South-East Crater (NSEC) studied here; distance from the EBEL station was ≈ 1 km. The Valle del Bove is a depression of spreading lava flows fed by the NSEC. Figure taken from Behncke et al. 2014
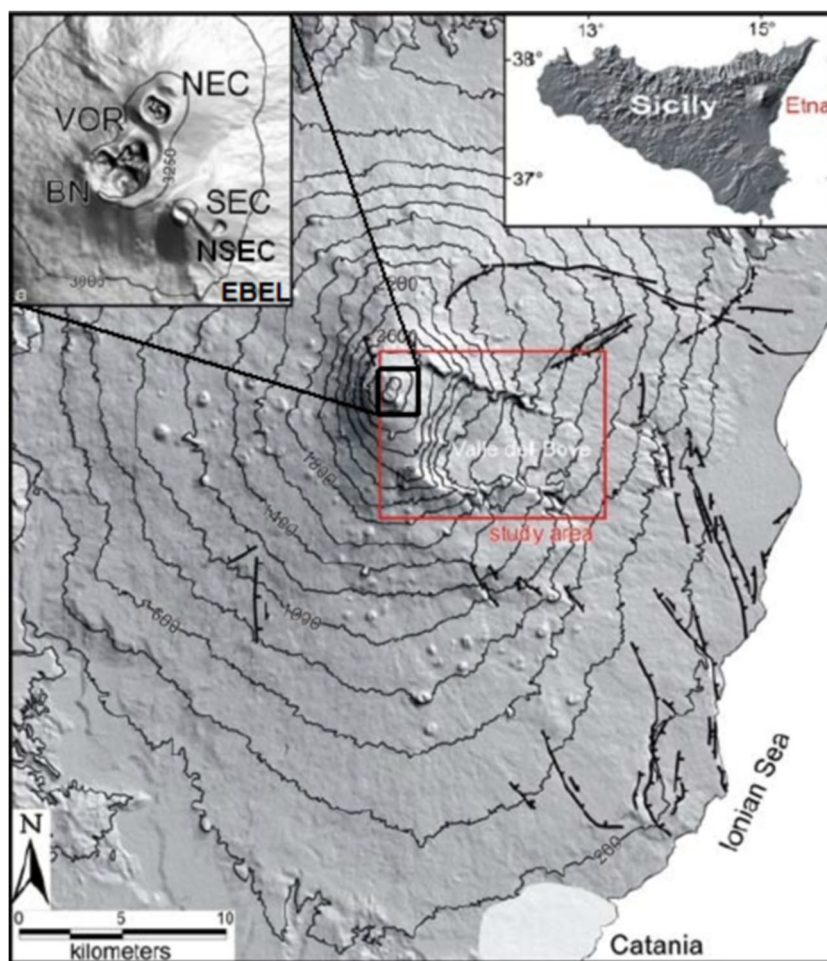
strombolian events within each whole data set, we needed to use a sliding window of 1000 samples in size (W_{cur}) to cover the data linearly. In the case of no activity, the radiometer will still record noise, this being environmental modifications such as solar reflection, clouds, vent puffing and fumarolic

Fig. 4 Example of the simulation of a radiometer field of view in thermal imagery (thermal image of North-East crater at Stromboli taken on 18 May 2014)

degassing from the crater rim. To correct for this noise, we needed to define the noise time span so as to calculate an average noise value. To do this, we computed the correlation coefficient (ρ_i) and the p Value (pVal$_i$) at time i, between smaller windows, these being $[i-50; i]$ and $[i; i+50]$. Empirically, we found that the noise time span corresponded to $W_{noise}=[k-50; k]$, with k being the smallest value of W_{cur} which gave $\rho_k>0.5$ and pVal$_k<0.05$. Once the noise is removed from the data, we can detect the beginning of each event from the point when a value switches from negative to positive, as well as the end (positive to negative). To define the event temporal conditions, we begin from the time ($t_{peakMax}$) of the maximum value ($T_{peakMax}$) and descend down both sides of the waveform until the switch conditions are reached. Now the beginning (t_{beg}) and the end (t_{end}) of the event can be defined.

Parameter computation

The temperature at the beginning (T_{beg}) and at the end (T_{end}) of the event was trivial to extract, these being the temperatures recorded at t_{beg} and t_{end}; as was the event duration

Fig. 5 Thermal waveforms for a lava fountain episode recorded at Mt. Etna on 4 March 2012 starting at 04:00 UT (**a**), an event detected during the precursory strombolian phase of the 4 March 2012 episode at 05:09 (**b**) and a normal explosion at Stromboli on 28 October 2012 (raw data in *blue*, SG$_0$ in *red*) (**c**)
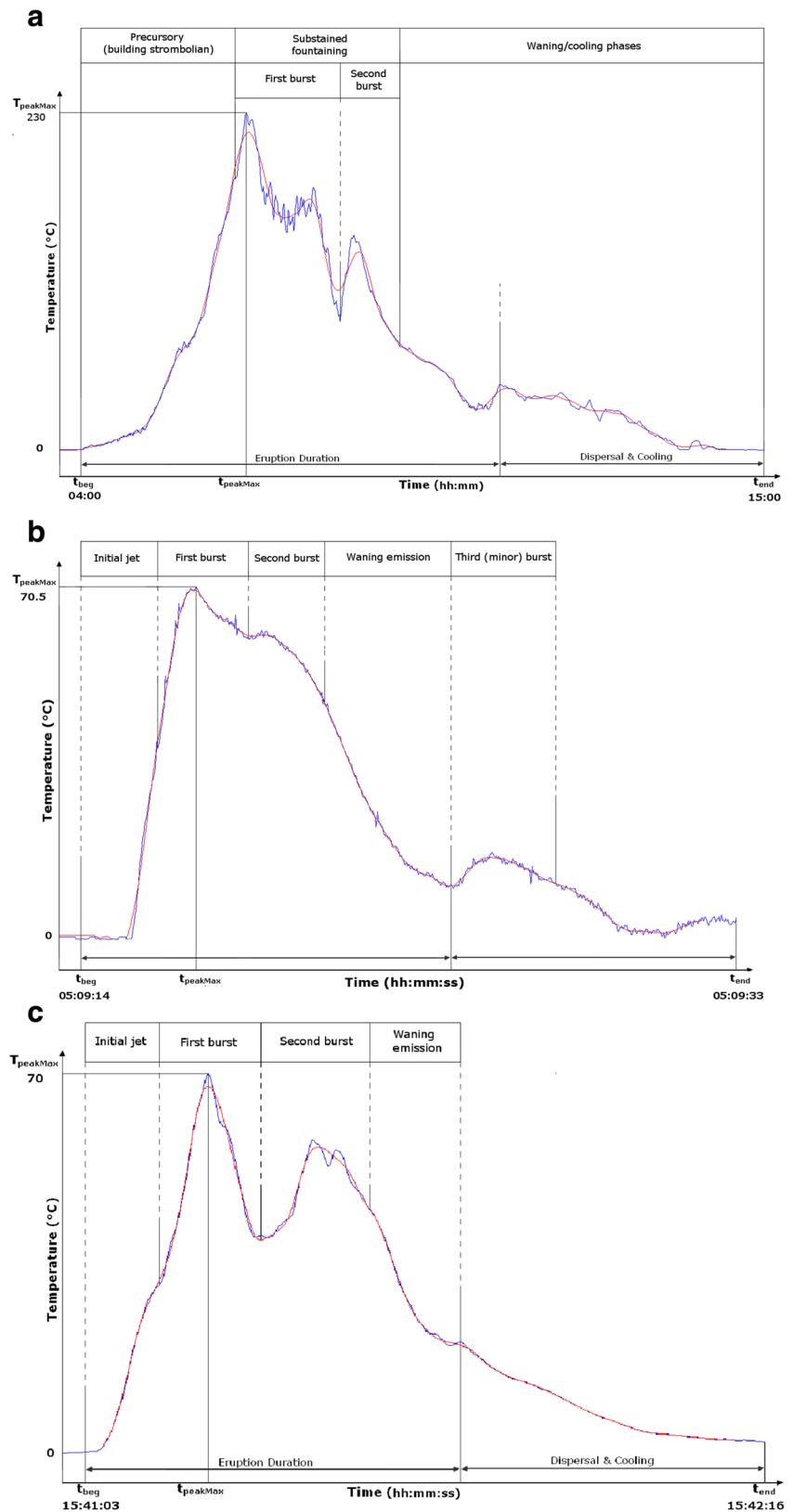
($t_{event} = t_{end} − t_{beg}$). By considering the difference in temperature between t_{beg} and $t_{peakMax}$, and the duration of the ascending ($t_{asc} = t_{peakMax} − t_{beg}$) and descending ($t_{desc} = t_{end} − t_{peakMax}$) limbs, we can also compute the slope of ascent $\left(S_{asc} = \frac{T_{peakMax} − T_{beg}}{t_{asc}}\right)$ and descent $\left(S_{desc} = \frac{T_{end} − T_{peakMax}}{t_{desc}}\right)$.

Next, we used a Savitzky-Golay filter (Savitzky and Golay 1964) to smooth the data (SG$_0$, the 0th derivative) and to estimate the derivatives of the smoothed signal (SGi being the i_{th} derivative). Visually, SG$_0$ is a perfect representation of the ideal strombolian waveform described by Harris (2013) and given here Fig. 5a. SG$_1$ values of zero provide us the local limits, these being either a local minimum or maximum point. We can also define the inflexion point as the point where SG$_2$ changes sign. The value of the function may not reach exact zero, so we search for a change in the sign to define the points surrounding the zero point of the function. Finally, the number of SG$_1$ maximum points will correspond to the number of bursts that comprise the event (N_{peaks}).

Now, we can compute the event radiant exitance (M_{rad}), the radiant flux (Φ_{rad}) and the radiant energy (Q_{rad}). The Stefan-Boltzmann law allows us to express the power radiated by a hot volcanic surface in terms of temperature [see Harris (2013) for full review]. This law is given by:

$$M_{rad} = \varepsilon \, \sigma \left(T^4 - T_o^4 \right) \tag{1}$$

where ε is the emissivity of the surface, T the temperature of the hot volcanic surface, T_o the temperature of the ambient environment into which the surface is radiating and σ is the Stefan-Boltzmann constant ($5.670373 \times 10^{-8} \, Wm^{-2} K^{-4}$). Because radiant exitance is the radiant flux emitted by a surface per unit area, we integrate the radiant exitance to obtain radiant flux:

$$\Phi_{rad} = \oint_{\Sigma} M_{rad} \, dA_{FOV} \tag{2}$$

Where A_{FOV} is the area of the emitting surface, i.e. the FOV of the radiometer. Given a complete thermal waveform for a volcanic event, such as emission of a hot cloud of gas and particles, radiant energy can now be calculated (e.g. Johnson et al. 2004; Sahetapy-Engel et al. 2008; Marchetti et al. 2009). Radiant energy is the radiant flux integrated through time, so that:

$$Q_{rad} = \int_{t_{beg}}^{t_{end}} \Phi_{rad} \, dt = \int_{t_{beg}}^{t_{end}} \oint_{\Sigma} \varepsilon \, \sigma \, T^4 dA_{FOV} dt \tag{3}$$

Now, for each event, we have 12 non-independent parameters based on temporal and thermal characteristics of the waveform that can be used to define its shape, energy and temporal evolution.

Results

We begin by considering a single fountaining episode from NSEC on 4 March 2012 which lasted 12 h. The following description is translated from INGV-OE Bollettino N°10 (2012). The episode began at 04:29 (all times are UTC) with an increase in the volcanic tremor amplitude and of strombolian explosion frequency and intensity. Shortly after 06:00, a lava flow spread in the direction of the western wall of the Valle del Bove (Fig. 3), while explosive activity continued to increase, with the climax and transition to fountaining occurring around 07:10. During this episode, the precursory strombolian phase lasted 2 h and 40 min, during which time the peak temperature recorded by the radiometer gradually waxed, with the system switching to sustained fountaining when climax temperature was reached (Fig. 5a). The waveform looks very much like that recorded in high-temporal resolution (SEVIRI) spectral radiance data (Calvari et al. 2011; Ganci et al. 2011), except the period of sustained activity is not obscured by the tephra plume ascending above the fountain. This phase involved two bursts and was followed by a waning period during which activity levels decreased, and hot deposits began to cool (Fig. 5a).

During the precursory phase of the fountaining episode, 278 events were detected by our radiometer system, meaning that, when time averaged, the event rate was 110 events per hour. Event durations ranged from 4 to 57 s with an average of 19 s (Table 1). The number of bursts detected during a single event ranged from 1 to 10 with an average of 3.5. The radiant energy emitted by individual events ranged from 7.0×10^6 to 4.9×10^8 J (average = 6.5×10^7 J), with the total energy released during the entire episode being 1.8×10^{10} J. Temporally, the number of peaks recorded in any one minute picked up from 2 to 4 per minute during the first hour, to 8–18 thereafter (Fig. 6a). In parallel with this, the duration of each event also ramped up (Fig. 6b), and the peak temperature underwent a systematic increase (Fig. 6c). Because all three of these parameters are integrated in the measure of radiant energy, the minute-by-minute plot of Q_{rad} collapses to a trend whereby there is a steady increase at a rate of 5.4×10^6 J per minute over the 2.67-hour-long phase of precursory strombolian activity (Fig.6d).

In total, we have data for seven other episodes, these being the lava fountain episodes of 18 March, 12 April and 24 April 2012, and those of 19, 21, 23 and 28 February 2013. Together, these episodes provided us a total of 1927 recorded events and 8537 peaks, with event counts ranging between 66 and 650 per episode, with an average of 241 events. In terms of average event duration, there was little difference between each year, durations ranging from 4 to 59 s in 2012 (average = 18 s) and 4 to 55 s (average = 21 s) in 2013 (Table 1). However, in terms of average number of events recorded (overview in Table 1), the 2012 episodes had more events (393) than those of 2013 (88), so that the average event frequency was greater in 2012 (39 events/h) than that in 2013 (13 events/h). Most events had radiant energies from 3.0×10^6 to 5.8×10^9 J, with an average of 1.0×10^8 J. The total energy of each episode was 1.3×10^{10} to 8.8×10^{10} J (average = 4.2×10^{10} J) in 2012 and 1.9×10^9 to 1.2×10^{10} J (average = 5.3×10^9 J) in 2013 (Table 1).

Of the explosions recorded by us at Stromboli using the thermal camera, explosion durations ranged from 25 to 73 s

Table 1 Comparison of temporal and energy-based parameters for Mt. Etna's lava fountain episodes recorded by the EBEL station in 2012 and 2013

Date (dd/mm/yy)	Number of events detected	Average duration (s)	Average radiant energy (J)	Total radiant energy (J)
04/03/12	278	19	6.5×10^7	1.8×10^{10}
18/03/12	650	13	5.1×10^7	1.3×10^{10}
12/04/12	257	18	7.9×10^7	5.1×10^{10}
23/04/12	389	20	2.3×10^8	8.8×10^{10}
19/02/13	66	21	1.3×10^8	1.2×10^{10}
21/02/13	85	21	2.9×10^7	1.9×10^9
23/02/13	85	20	3.5×10^7	3.0×10^9
28/02/13	116	23	3.7×10^7	4.4×10^9

with an average of 48 s. This is a little longer than explosion durations typically recorded at Stromboli, which range from 4 to 30 s, with a mean duration of ~8 s (Hort et al. 2003; Harris and Ripepe 2007a; Patrick et al. 2007; Ripepe et al. 2008). However, the longer duration of the explosions examined here for Stromboli, mean that explosion durations were closer to the median event duration recorded at Etna. The number of bursts detected during a single explosion recorded at Stromboli ranged between one and two. The radiant energy ranged from 2.1 to 6.0×10^8 J, with an average of 3.2×10^8 J. We note that even if the duration for explosions at Stromboli was longer, on average, than duration for events at Mt. Etna, the average radiant energy was lower.

Our analysis indicates that some combination of our measured parameters is key in triggering the transition to sustained fountaining. To understand which combination, we plotted all of the data for all parameters in a three-dimensional space. Visualisation of multi-dimensional data is a challenge, and many techniques have been proposed to allow effective data visualisation (see Oliveira and Levkowitz (2003) for review). Here, we use a variation of the stochastic neighbour embedding method named *t*-SNE (Van der Maaten and Hinton 2008) that visualises multi-dimensional data by giving each event a

location in three-dimensional space. *T*-SNE is a nonlinear dimension-reduction technique, which aims to present the topology of large, multi-dimensional and nonlinear data sets with a high number of dimensions as a lower, but still meaningful, number of dimensions to allow visualisation and classification of links, relationships and trends. We here assume that events, represented by their thermal and temporal parameters, lie on a manifold with a very low number of dimensions (two or three). *T*-SNE allows definition of this manifold (plotting as a line in 3D and represented on a 3-axis plot in Fig. 7) and then projects events onto it allowing analysis of the temporal distribution of these events and the properties of the distribution. Figure 7 represents the manifold computed by *t*-SNE. The events lie on a roughly helicoidal path (Fig. 7a) ending in a sink (Fig. 7b). This well-defined trend implies that there is a relatively low dimensionality in our parameter set, and the elongate nature of the structure represents accumulation of energy during the transition phase, with black markers being the events of the weakest energy; red the highest. While a sink attracts all of the weak energy events, the highest energies lie along a path which extends from the sink to the highest energy event. In fact, as we move along the path away from the sink all event components (thermal energy, peak intensity,
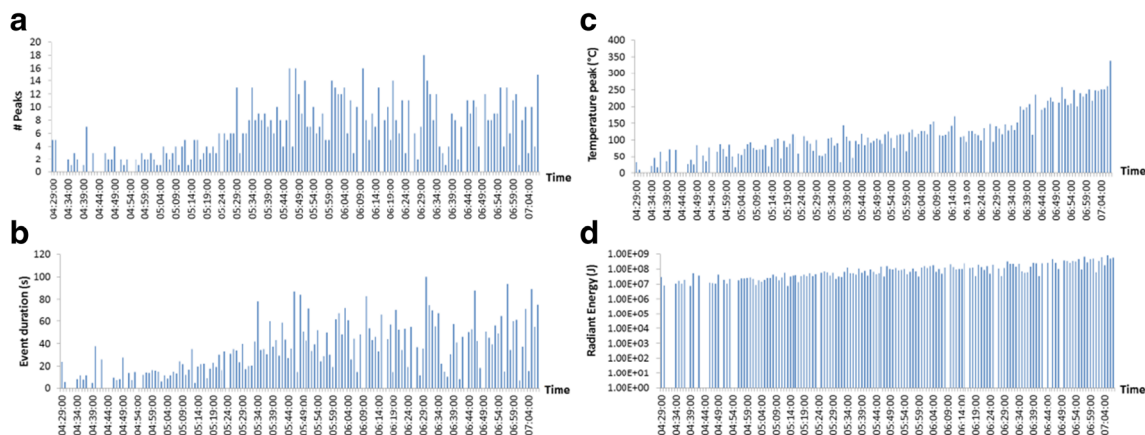

Fig. 6 Evolution of characteristic parameters of the lava fountain episode recorded at Mt. Etna on 4 March 2012 such as number of peaks (**a**), event duration (**b**), peak temperature (**c**) and radiant energy (**d**) trough time, in one minute bins

number of peaks, duration and/or radiance exitance) increase. If we plot events with temporal markers, events early in each episode (black circles in Fig. 7a) are part of the sink, but later events (red circles in Fig.7a) form the path; the highest energy events being those furthest from the sink. This supports a process whereby event energy increases over six orders of magnitude during the period of precursory strombolian activity, to culminate in the phase of sustained fountaining. If we complete a rank order analysis of all our event energies (Pyle 1998), we find that the lower limit of the system is at an energy of 2.9×10^6 J (Fig. 8). This is the typical value of the sink events meaning that the sink represents many similar, but weak (the lowest energy possible), events. As we move up the path and away from the sink, events become stronger (more energetic) (Fig.7b). The threshold for an event to be just beyond the path terminous is close to 10^7 J. Our rank order analysis predicts that the highest possible event we can expect is 8.1×10^9 J.

Discussion

For the precursory phases of the eight fountain episodes considered here, we count between 13 and 110 events per hour during the period prior to sustained fountaining. This is much less than the number of individual strombolian events recorded at Mt. Etna during the build-up to sustained fountaining, which typically ranges from 10 to 30 bursts per minute (Harris and Neri 2002; Vergniolle and Ripepe 2008; Calvari et al. 2011; Ulivieri et al. 2013). These rates are more consistent with what we here term "peaks" which, for example, increased to a rate of up to 18 per minute just prior to the period of sustained fountaining of 4 March 2012 (Fig. 6a). Thus, we distinguish between bursts, which are here represented by spikes in our waveform which are counted as individual peaks, and events which are composed of multiple (>1) individual bursts. Events are thus longer period oscillations during which the plume heat flux emitted by all single bursts that comprise the event, waxes and wanes. In effect, each event can be made up of multiple bursts (e.g. Spampinato et al. 2012 and Fig. 5b). This waveform looks much like those derived from radiometer-derived waveforms for paroxysmal explosions at Stromboli (Rosi et al. 2006; Harris et al. 2008), as well as that derived by us from the thermal camera data acquired during normal explosive activity (Fig. 5c). In the case of Stromboli, each peak within the explosion waveform is associated with renewed emission of hot gas and particles; each of which relates to a discrete gas burst that carries with it fragments of magma that had been residing in the upper conduit (Gurioli et al. 2014; Leduc et al. 2015). The number, duration and intensity of each burst within the event then combine to determine the event magnitude, as here described by the event radiant energy.

In Fig. 9, we assess event shape in terms of the following normalised shape index: $(S_{asc} - S_{desc}/S_{asc} + S_{desc})$. Using this index, an event waveform with little or no waning phase will have a positive value whereas an impulsive event with a long-waning phase will have a negative value; a symmetric waveform will have a value of 0. We found that 1508 (78 %) of our events had a short waxing phase with a dominant waning phase. Of the remaining events, 313 (16 %) had waning phases that were shorter than the waxing phase, and 112 (6 %) were symmetric. The 313 events that had short-waning phases were typically found later in the episode, around 3.4 h after the beginning of the first event. This is consistent with events developing from complex "long-waning", events involving multiple bursts of decaying intensity, to "short-waning" events involving single bursts. This tendency is enhanced by the increased burst frequency prior to the transition to sustained fountaining, so that the waxing-limb of the following event overprints, and thus prematurely terminates, the waning-limb of the preceding event.

We can thus say that climax was reached, on average, 3.4 h after the beginning of the first event, during which time the thermal event duration, maximum temperature and thermal energy all steadily increased. These thermal events are thus precursors to sustained fountaining, where we find that the transition to fountaining involves crossing over a thermal energy threshold of 10^9 J, with a maximum possible event energy being 10^{10} J. The lowest energies are 10^6 J and are needing to exceed a threshold of 10^7 J to begin the path out of the sink and towards sustained fountaining. These energies compare with 10^8 J obtained for normal explosive activity at Stromboli, indicating that each fountaining episode begins with events that are weaker than explosions typically observed at Stromboli. This is the case until around one hour and 15 min into the episode, when events exceed 10^8 J.

Our trend in event energy is consistent the activity sequence commonly observed during Mount Etna's lava fountaining episodes, during which strombolian events are discrete and well separated in time at the beginning of the episode, but become more and more frequent as the climax approaches (e.g. Calvari et al. 2011; Spampinato et al. 2012). Likewise, Vergniolle and Ripepe's (2008) infrasonic data for two fountaining episodes at Etna in 2001 revealed an evolution from a low frequency (one burst every few minutes) of weak strombolian events minutes to a higher frequency (one every ~8 s) of stronger events during fountaining when sustained "infrasonic tremor" is recorded (Cannata et al. 2009). During this evolution of activity style, the degassing regime and flux changes (from slug flow to churn flow) and increases (e.g. Greenland et al. 1988; Parfitt and Wilson 1995; Parfitt et al. 1995; Parfitt 2004; Polacci et al. 2006; Ulivieri et al. 2013; Pioli et al. 2012). Thus, we may relate our increasing trend in event thermal energy to increasing volumes of gas arriving and bursting at the
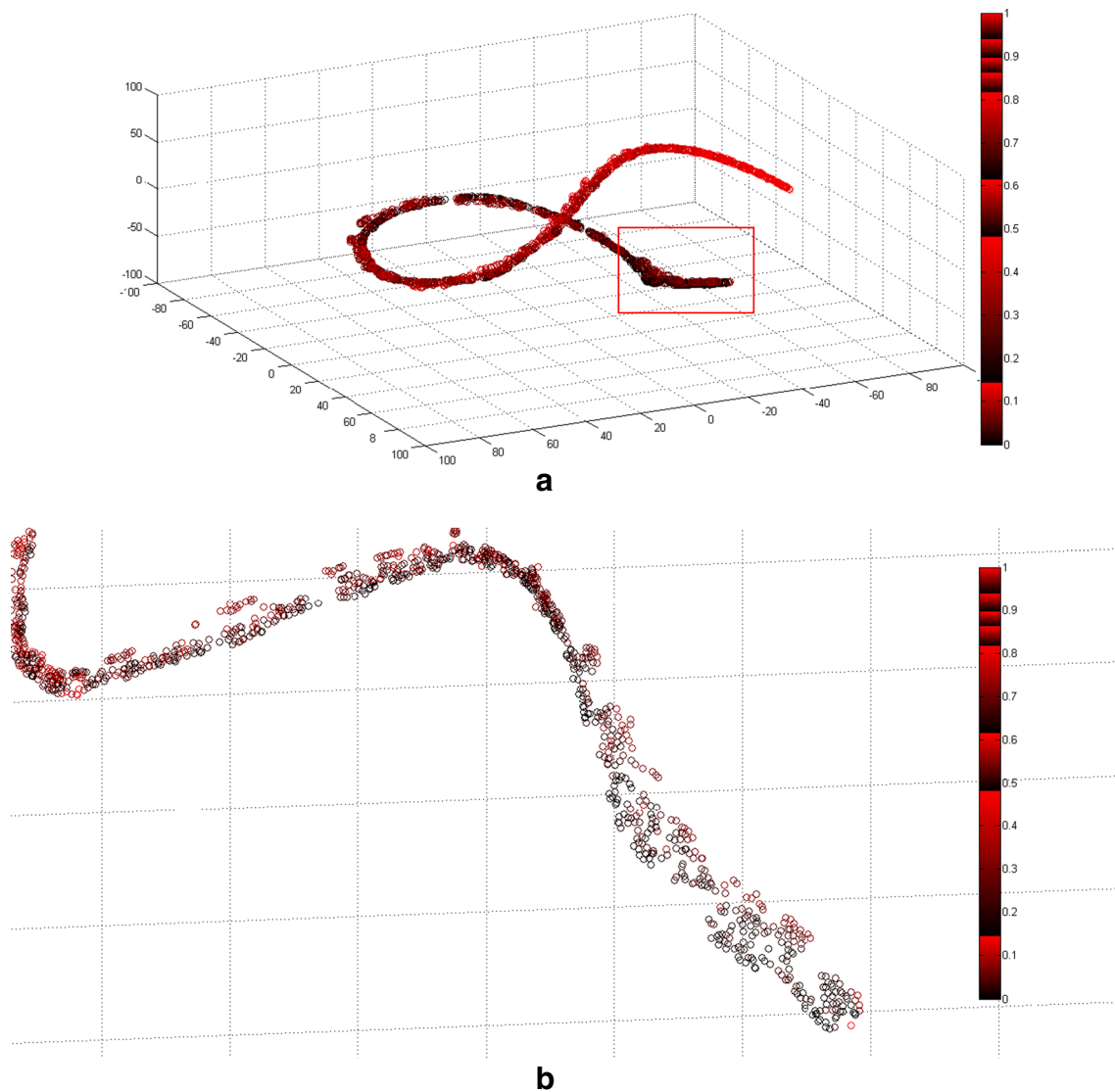
a

b

Fig. 7 Visual representation of the times and energies of events recorded at Mt. Etna. Each event is represented by a coloured circle. Colours are representatives of the chronology of the episode (early in *black*, late in *red*). From 0 to 1, bins represent the different episodes. The manifold presents an approximately helicoidal shape (**a**) ending in a sink at which the weaker events are represented (**b**). Axes cannot be defined because the *t*-SNE algorithm is a nonlinear dimensionality reduction technique that visualises multi-dimensional data by giving each event a location in a three-dimensional space in which similar parameters are statistically attracted to each other, and dissimilar parameters are separated. To do this, first, the *t*-SNE generates a probability surface. In many ways, this is a large-scale analogue of gas-pistoning, whereby the frequency of bubble bursting increases over a period of several minutes to tens of minutes, until a sustained gas jet punches through the magma free-surface to re-set the cycle of hiatus, bubble bursting and jetting (Johnson et al. 2004; Marchetti and Harris 2008). It is striking that the shape and proportions of the waveform for the entire fountaining episode (Fig 5a) are the same as those of the waveforms that comprise the component events distribution by converting the high-dimensional Euclidean distances between data points in such way that the more data points are similar, the higher the probability of being selected. The same process is completed over the points in the low-dimensional space using a heavy-tailed Student's t-distribution. Second, the algorithm minimises a symmetrical Kullback-Leibler divergence between the two joint probability distributions using a gradient descent method. Taken together, *t*-SNE separates dissimilar data points by means of large pairwise distances, and brings similar data points closer together by assigning them small pairwise distances. That is, the first test causes convergence; the second divergence

(Fig 5b). These have, in turn, the shape and proportionality of the waveform derived for the normal explosion at Stromboli (Fig 5c). Thus, we suggest that all the three wave-forms are related to the same degassing processes, which involve multiple releases of large slugs of pressurised gas which carry with them fragments entrained from the magma resident in the conduit through which the gas ascends.
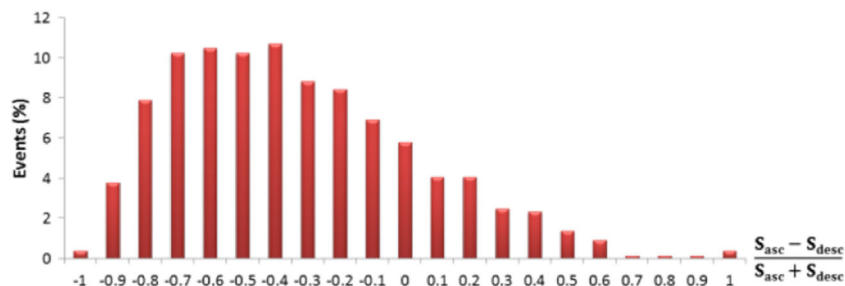
Statistically, the events of 2012 were of higher magnitude and intensity than in 2013, having an average

Fig. 8 Rank order plot for all event radiances. The strongest events tend toward an asymptote representative of the upper limit near E +10, while the weakest events, near E +6 indicate the lower limit to the system
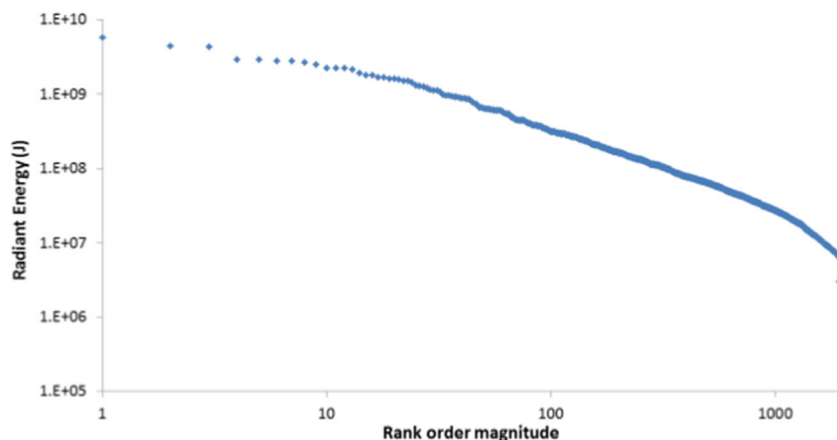
thermal energy 5×10^7 J greater than those recorded in 2013. Although event durations were similar during the two years, the average number of events was greater in 2012, being 394 as opposed to 88 in 2013. This indicates a decrease in the magnitude and intensity of the fountaining activity between the two years. It also points to a change in style of the activity, whereby although event duration remained the same, their frequency and thermal energy diminished. This could indicate a decrease in the flux of gaseous and solid material involved in each event. Fountains at Mt. Etna have been interpreted in terms of fast ascent of gas-rich batches from the deep source (Harris and Neri 2002) or due to collapse of foam collecting in a shallow holding chamber (e.g. Allard et al. 2005). Either way, the amount of gas rising or accumulating prior to each fountaining episode appears to have diminished, thus explaining the change in intensity, magnitude and style. This is consistent with the degassing model of Vergniolle and Gaudemer (2012) which explains cycles of degassing, fire-fountaining to effusive activity to changes in the degassing regime. It is of note that, after our study, Mt. Etna witnessed two effusive episodes which, given our results, appear to have been heralded by a decrease in the intensity of fountaining episodes (Gambino et al. 2016, in review).

Conclusions

We developed an algorithm to compute radiometer-derived parameters during the precursory phase to sustained fountaining, such as event duration, length of waxing/waning phases, number of peaks comprising each event, event intensity (peak energy) and event radiant energy. This allows automated tracking of strombolian events using a near-real time feed of radiometer data. The deployment of the radiometer allows thermal observations with a low-cost (expendable) instrument from safe, remote, locations, yielding thermal data that allow episode characterisation and tracking. Interestingly, if we want to find a pattern or trend in the build-up phase to sustained fountaining at Etna, it is the strombolian events that we have to consider, not the individual bursts. Each event comprises multiple individual bursts of gas and particles, each of whose emitted radiances are integrated across the entire event cluster. It is thus not the frequency or thermal intensity of single bursts that we track, but instead the thermal energy of each event, which is a function of the frequency of bursts in each cluster, and each burst's thermal intensity and duration.

Using our statistically robust data set, we are thus able to define thermal thresholds that mark the transition to sustained fountaining, as well as the point at which the energy of precursory events begins to increase away from those of the initial low-energy onset event. For our case, we find that

Fig. 9 Shape distribution of the events detected in the whole data set (four episodes in 2012 and four episodes from 2013). Most of the events have a short waxing phase and a dominant waning phase

fountaining episodes evolve from into a steadily increasing event frequency and thermal energy trend from a thermally defined define an onset phase (when energies are less than 10^7 J). Event energies then progress along a path until the case-specific threshold of 5.0×10^9 J is reached, and the system trips to sustained fountaining; this can occur over a period of a few minutes.

These energy thresholds must be defined for each given radiometer distance or angular field of view. If, for example, we moved our radiometer back 5 km the effects of atmosphere and the presence of cold sky in the background would change the FOV-integrated radiance. Thus, to be applicable to other basaltic systems, we need to define these thresholds on a case-by-case basis depending on the size and location of the radiometer field of view. However, for any stable instrument-target geometry, relative changes are a trustworthy and reliable measure of event energy.

References

Aksakal SK (2013) Geometric accuracy investigations of SEVIRI High-Resolution Visible (HRV) level 1.5 imagery. Remote Sens 5:2475–2491. doi:10.3390/rs5052475

Allard P, Burton M, Murè F (2005) Spectroscopic evidence for a lava fountain driven by previously accumulated magmatic gas. Nature 433(7024):407–410. doi:10.1038/nature03246

Aloisi M, D'Agostino M, Dean KG, Mostaccio A, Neri G (2002) Satellite analysis and PUFF simulation of the eruptive cloud generated by the Mount Etna paroxysm of 22 July 1998. J Geophys Res 107(B12): 2373. doi:10.1029/2001JB000630

Andronico D, Cristaldi A, Scollo S (2008) The 4–5 September 2007 lava fountain at South-East Crater of Mt Etna, Italy. J Volcanol Geotherm Res 173:325–328. doi:10.1016/j.jvolgeores.2008.02.004

Behncke B, Neri M, Pecora E, Zanon V (2006) The exceptional activity and growth of the Southeast Crater, Mount Etna (Italy), between 1996 and 2011. Bull Volcanol. doi:10.1007/s00445-006-0061-x

Behncke B, Branca S, Corsaro RA, De Beni E, Miraglia L, Proietti C (2014) The 2011–2012 summit activity of Mount Etna: birth, growth and products of the new SE crater. J Volcanol Geotherm Res 270:10–21. doi:10.1016/j.jvolgeores.2013.11.012

Bertrand C, Clerbaux N, Ipe A, Gonzalez L (2003) Estimation of the 2002 Mount Etna eruption cloud radiative forcing from Meteosat-7 data. Remote Sens Environ 87:257–272

Bertrand PR, Fhima M, Guillin A (2011) Off-line detection of multiple change points by the filtered derivative with p-value method. Seq Anal 30(2):172–207. doi:10.1080/07474946.2011.563710

Bombrun M, Harris A, Gurioli L, Battaglia J, Barra V (2015a) Anatomy of a strombolian eruption: inferences from particle data recorded with thermal video. J Geophys Res 120(4):2367–2387. doi:10.1002/2014JB011556

Bombrun M, Barra V, Harris A (2015b) Analysis of thermal video for coarse to fine particle tracking in volcanic explosion plumes. In Image Analysis (pp. 366–376). Springer International Publishing, doi: 10.1007/978-3-319-19665-7_30

Bonaccorso A, Caltabiano T, Currenti G, Del Negro C, et al. (2011) Dynamics of a lava fountain revealed by geophysical, geochemical and thermal satellite measurements: The case of the 10 April 2011 Mt Etna eruption. Geophys Res Lett 38(24): doi:10.1029/2011GL049637

Bonaccorso A, Calvari S, Currenti G, Del Negro C, Ganci G, Linde A, Napoli R, Sacks S, Sicali A (2013a) From source to surface: dynamics of Etna's lava fountains investigated by continuous strain, magnetic, ground and satellite thermal data. Bull Volcanol 75 (690): doi: 10.1007/s00445-013-0690-9

Bonaccorso A, Currenti G, Linde A, Sacks S (2013b) New data from borehole strainmeters to infer lava fountain sources (Etna 2011–2012). Geophys Res Lett 40:3579–3584. doi:10.1002/grl.50692

Branan YK, Harris A, Watson IM, Phillips JC, Horton K, Williams-Jones G, Garbeil H (2008) Investigation of at-vent dynamics and dilution using thermal infrared thermometers at Masaya Volcano, Nicaragua. J Volcanol Geotherm Res 169:34–47. doi:10.1016/j.jvolgeores.2007.07.021

Calvari S, Salerno GG, Spampinato L, Gouhier M, La Spina A, Pecora E, Harris AJL, Labazuy P, Biale E, Boschi E (2011) An unloading foam model to constrain Etna's 11–13 January 2011 lava fountaining episode. J Geophys Res 116:B11207. doi:10.1029/2011JB008407

Cannata A, Montalto P, Privitera E, Russo G, Gresta S (2009) Tracking eruptive phenomena by infrasound: May 13, 2008 eruption at Mt. Etna. Geophys Res Lett 36:L05304. doi:10.1029/2008GL036738

Gambino S, Cannata A, Cannavò F, La Spina A, Palano M, Sciotto M, Spampinato L, Barberi G 2016 The unusual December 28, 2014 dyke-fed paroxysm at Mt. Etna: timing and mechanism from a multidisciplinary perspective. J Geophys Res. In review

Ganci G, Vicari A, Bonfiglio S, Gallo G, Del Negro C (2011) A text onbased cloud detection algorithm for MSG-SEVIRI multispectral images. Geomatics Nat Haz Risk 2:1–12. doi:10.1080/19475705.2011.578263

Ganci G, Harris AJL, Del Negro C, Guéhenneux Y, Cappello A, Labazuy P, Calvari S, Gouhier M (2012) A year of lava fountaining at Etna: volumes from SEVIRI. Geophys Res Lett 39:L06305. doi:10.1029/2012GL051026

Ganci G, James MR, Calvari S, Del Negro C (2013) Separating the thermal fingerprints of lava flows and simultaneous lava fountaining using ground-based thermal camera and SEVIRI measurements. Geophys Res Lett 40:5058–5063. doi:10.1002/grl.50983

Gouhier M, Harris AJL, Calvari S, Labazuy P, Guéhenneux Y, Donnadieu F, Valade S (2012) Lava discharge during Etna's January 2011 fire fountain tracked using MSG-SEVIRI. Bull Volcanol 74:787–793. doi:10.1007/s00445-011-0572-y

Greenland LP, Okamura AT, Stokes JB (1988) Constraints on the mechanisms of the eruption. US Geol Surv Prof Pap 1463:155–164

Gurioli L, Colò L, Bollasina AJ, Harris AJL, Whittington A, Ripepe M (2014) Dynamics of strombolian explosions: inferences from field and laboratory studies of erupted bombs from Stromboli volcano. J Geophys Res: Solid Earth 119(1):319–345. doi:10.1002/2013JB010355

Harris AJL, Neri M (2002) Volumetric observations during paroxysmal eruptions at Mount Etna: pressurized drainage of a shallow chamber or pulsed supply? J Volcanol Geotherm Res 116(1):79–95. doi:10.1016/S0377-0273(02)00212-3

Harris AJL, Ripepe M (2007a) Synergy of multiple geophysical approaches to unravel explosive eruption conduit and source

dynamics—a case study from Stromboli. Chem Erde 67:1–35. doi: 10.1016/j.chemer.2007.01.003

Harris A, Ripepe M (2007b) Temperature and dynamics of degassing at Stromboli. J Geophys Res 112:B03205. doi:10.1029/2006JB004393

Harris AJL, Stevens NF, Maciejewski AJH, Röllin PJ (1996) Thermal evidence for linked vents at Stromboli. Acta Vulcanol 8:57–62

Harris A, Johnson J, Horton K, Garbeil G, Pirie D, Ramm H, Donegan S, Pilger E, Flynn L, Mouginis-Mark P, Ripepe M, Marchetti E, Rothery D (2003) Ground-based infrared monitoring provides new tool for remote tracking of volcanic activity. Eos 84(40):409–418

Harris A, Pirie D, Horton K, Garbeil H, Pilger E, Ramm H, Hoblitt R, Thornber C, Ripepe M, Marchetti E, Poggi P (2005) DUCKS: low cost thermal monitoring units for near-vent deployment. J Volcanol Geotherm Res 143:335–360. doi:10.1016/j.jvolgeores.2004.12.007

Harris AJL, Ripepe M, Calvari S, Lodato L, Spampinato L (2008) The 5 April 2003 explosion of Stromboli: timing of eruption dynamics using thermal data. AGU Geophys Monograph 182:305–316. doi: 10.1029/182GM25

Harris AJL, Valade S, Sawyer GM et al (2013a) Modern multispectral sensors help track explosive eruptions. Eos Trans Am Geophys Union 94(37):321–322. doi:10.1002/2013EO370001

Harris AJL, Delle Donne D, Dehn J, Ripepe M, Worden K (2013b) Volcanic plume and bomb field masses from thermal infrared camera imagery. Earth Planet Sci Lett 365:77–85. doi:10.1016/j.epsl.2013.01.004

Harris AJL (2013) Thermal remote sensing of active volcanoes: a user's manual. Cambridge University Press. Cambridge, UK, 728 p

Heliker C, Mattox TN (2003) The first two decades of the PuʻuʻŌʻō-Kūpaianaha eruption: chronology and selected bibliography. US Geol Surv Prof Pap 1676:1–27

Hort M, Seyfried R, Voge M (2003) Radar Doppler velocimetry of volcanic eruptions: theoretical considerations and quantitative documentation of changes in eruptive behaviour at Stromboli volcano, Italy. Geophys J Int 154:515–532

Houghton BF, Gonnermann HM (2008) Basaltic explosive volcanism: constraints from deposits and models. Chem Erde 68:117–140. doi:10.1016/j.chemer.2008.04.002

INGV-OE (2012) Bollettino settimanale sul monitoraggio vulcanico, geochimico e sismico del vulcano Etna: 27/02/2012 - 04/03/2012

Johnson JB, Harris AJL, Sahetapy-Engel S, Wolf RE, Rose WI (2004) Explosion dynamics of vertically-directed pyroclastic eruptions at Santiaguito, Guatemala. Geophys Res Lett 31:L06610

Johnson JB, Harris AJL, Hoblitt R (2005) Thermal observations of gas pistoning at Kilauea Volcano. J Geophys Res 110:B11201. doi:10.1029/2005JB003944

Leduc L, Gurioli L, Harris A, Colò L, Rose-Koga EF (2015) Types and mechanisms of strombolian explosions: characterization of a gas-dominated explosion at Stromboli. Bull Volcanol 77(1):1–15. doi:10.1007/s00445-014-0888-5

Marchetti E, Harris AJL (2008) Trends in activity at Pu'u 'O'o during 2001–2003: insights from the continuous thermal record. Geol Soc, London, Special Publication 307: 85–101 doi:10.1144/SP307.6

Marchetti E, Ripepe M, Harris AJL, Delle Donne D (2009) Tracing the differences between Vulcanian and Strombolian explosions using infrasonic and thermal radiation energy. Earth Planet Sci Lett 279:273–281. doi:10.1016/j.epsl.2009.01.004

Mercalli G (1907) I vulcani attivi della Terra. Ulrico Hoepli (Milano): 422 p

Murè F, Larocca G, Spampinato L, Caltabiano T, Salerno GG, Montalto P, Scuderi L (2013) Installazione di un radiometronell'area sommitale delvulcano Etna. Rapporti Tecnici INGV

Newhall CG, Self S (1982) The volcanic explosivity index (VEI): an estimate of explosive magnitude for historical volcanism. J Geophys Res 87:1231–1238. doi:10.1029/JC087iC02p01231

Oliveira MCF, Levkowitz H (2003) From visual data exploration to visual data mining: a survey. IEEE Trans Vis Comput Graph 9(3):378–394. doi:10.1109/TVCG.2003.1207445

Patrick MR, Harris AJL, Ripepe M, Dehn J, Rothery DA, Calvari S (2007) Strombolian explosive styles and source conditions: insights from thermal (FLIR) video. Bull Volcanol 69(7):769–784. doi:10.1007/s00445-006-0107-0

Patrick MR (2007) Dynamics of strombolian ash plumes from thermal video: motion, morphology, and air entrainment. J Geophys Res 112(B6): doi:10.1029/2006JB004387

Parfitt EA (2004) A discussion of the mechanisms of explosive basaltic eruptions. J Volcanol Geotherm Res 134:77–107

Parfitt EA, Wilson L (1995) Explosive volcanic eruptions. IX: the transition between Hawaiian-style lava fountaining and strombolian explosive activity. Geophys J Int 121:226–232

Parfitt EA, Wilson L, Neal CA (1995) Factors influencing the height of Hawaiian lava fountains: implications for the use of fountain height as an indicator of magma gas content. Bull Volcanol 57:440–450

Pioli L, Rosi M, Calvari S, Spampinato L, Renzulli A, Di Roberto A (2008) The eruptive activity of 28 and 29 December 2002. Am Geophys Union Monog 182:105–116. doi:10.1029/182GM10

Pioli L, Bonadonna C, Azzopardi BJ, Phillips JC, Ripepe M (2012) Experimental constraints on the outgassing dynamics of basaltic magmas. J Geophys Res 117:B03204. doi:10.1029/2011JB008392

Polacci M, Corsaro RA, Andronico D (2006) Coupled textural and compositional characterization of basaltic scoria: insights into the transition from strombolian to fire fountain activity at Mount Etna, Italy. Geology 34:201–204. doi:10.1130/G22318.1

Pyle DM (1998) Forecasting sizes and repose times of future extreme volcanic events. Geology 26(4):367–370. doi:10.1130/0091-7613

Ramsey MS, Harris AJL (2013) Volcanology 2020: how will thermal remote sensing of volcanic surface activity evolve over next decade? J Volcanol Geotherm Res 249:217–233. doi:10.1016/j.jvolgeores.2012.05.011

Ripepe M, Harris AJL (2008) Dynamics of the 5 April 2003 explosive paroxysm observed at Stromboli by a near-vent thermal, seismic and infrasonic array. Geophys Res Lett 35:L07306. doi:10.1029/2007GL032533

Ripepe M, Harris AJL, Carniel R (2002) Thermal, seismic and infrasonic evidences of variable degassing rates at Stromboli volcano. J Volcanol Geotherm Res 118:285–207. doi:10.1016/S0377-0273(02)00298-6

Ripepe M, Marchetti E, Poggi P, Harris AJL, Fiaschi A, Ulivieri G (2004) Seismic, acoustic, and thermal network monitors the 2003 eruption of Stromboli volcano. Eos 85(35):329–332. doi:10.1029/2004EO350001

Ripepe M, Harris AJL, Marchetti M (2005) Coupled thermal oscillations in explosive activity at different craters of Stromboli volcano. Geophys Res Lett 32:L17302. doi:10.1029/2005GL022711

Ripepe M, Delle Donne D, Harris A, Marchetti M, Ulivieri G (2008) Dynamics of strombolian activity. AGU Geophys Monog 182:39–48. doi:10.1029/182GM05

Rosi M, Bertagnini A, Harris AJL, Pioli L, Pistolesi M, Ripepe M (2006) A case history of paroxysmal explosion at Stromboli: timing and dynamics of the April 5, 2003 event. Earth Planet Sci Lett 243:594–606

Sahetapy-Engel ST, Harris AJL, Marchetti E (2008) Thermal, seismic and infrasound observations of persistent explosive activity and conduit dynamics at Santiaguito Lava Dome, Guatemala. J Volcanol Geotherm Res 173:1–14. doi:10.1016/j.jvolgeores.2007.11.026

Savitzky A, Golay MJ (1964) Smoothing and differentiation of data by simplified least squares procedures. Anal Chem 36(8):1627–1639. doi:10.1021/ac60214a047

Sciotto M, Rowe CA, Cannata A, Arrowsmith S, Privitera E, Gresta S (2011) Investigation of volcanic seismo-acoustic signals: applying

subspace detection to lava fountain activity at Etna Volcano. AGU Fall Meet Abstracts 1:2685

Shimozuru D (1971) Observation of volcanic eruption by an infrared radiation meter. Nature 234:457–459. doi:10.1038/234457a0

Spampinato L, Calvari S, Oppenheimer C, Lodato L (2008) Shallow magma transport for the 2002–3 Mt Etna eruption inferred from thermal infrared surveys. J Volcanol Geotherm Res 177:301–312

Spampinato L, Oppenheimer C, Cannata A, Montalto P, Salerno GG, Calvari S (2012) On the time-scale of thermal cycles associated with open-vent degassing. Bull Volcanol 74(6):1281–1292. doi:10.1007/s00445-012-0592-2

Spampinato L, Sciotto M, Cannata A, Cannavò F et al (2015) Multi-parametric study of the February–April 2013 paroxysmal phase of Mt. Etna. New South-East crater, Geochemistry, Geophysics, Geosystems. doi:10.1002/2015GC005795

Stovall WK, Houghton BF, Gonnermann H, Fagents SA, Swanson DA (2010) Eruption dynamics of Hawaiian-style fountains: the case study of episode 1 of the Kilauea Iki 1959 eruption. Bull Volcanol. doi:10.1007/s00445-010-0426-z

Swanson DA, Duffield WA, Jackson DB, Peterson DB (1979) Chronological narrative of the 1969–1971 Mauna Ulu eruption of Kilauea volcano, Hawaii. US Geol Surv Prof Pap 1056:1–59

Van der Maaten L, Hinton G (2008) Visualizing data using t-SNE. J Mach Learn Res 9:2579–2605

Vergniolle S, Gaudemer Y (2012) Decadal evolution of a degassing magma reservoir unravelled from fire fountains produced at Etna volcano (Italy) between 1989 and 2001. Bull Volcanol 74(3):725–742. doi:10.1007/s00445-011-0563-z

Vergniolle S, Mangan M (2000) Hawaiian and strombolian eruptions. In: Sigurdsson H. (ed.), Encyclopedia of Volcanoes (Academic Press): p. 447–461

Vergniolle S, Ripepe M (2008) From strombolian explosions to fire fountains at Etna Volcano (Italy): what do we learn from acoustic measurements? Geological Society London Special Publication 307: 103–124 doi:10.1144/SP307.7

Ulivieri G, Ripepe M, Marchetti E (2013) Infrasound reveals transition to oscillatory discharge regime during lava fountaining: implication for early warning. Geophys Res Lett 40:3008–3013. doi:10.1002/grl.50592

Wolff JA, Sumner JM (2000) Lava fountains and their products. In: Sigurdson, H. (ed.), Encyclopedia of Volcanoes (Academic Press): pp 321–329

Wolfe EW, Neal CA, Banks NG, Duggan TJ (1988) Geologic observations and chronology of eruptive events. US Geol Surv Prof Pap 1463:1–97

Zettwoog P, Tazieff H (1972) Instrumentation for measuring and recording mass and energy transfer from volcanoes to atmosphere. Bull Volcanol 36(1):1–19. doi:10.1007/BF02596979